



The Ice, Cloud, and land Elevation Satellite-2 (ICESat-2): Science requirements, concept, and implementation



Thorsten Markus^{a,*}, Tom Neumann^a, Anthony Martino^a, Waleed Abdalati^b, Kelly Brunt^{a,c}, Beata Csatho^d, Sinead Farrell^c, Helen Fricker^e, Alex Gardner^f, David Harding^a, Michael Jasinski^a, Ron Kwok^f, Lori Magruder^g, Dan Lubin^e, Scott Luthcke^a, James Morison^h, Ross Nelson^a, Amy Neuenschwander^g, Stephen Palm^a, Sorin Popescuⁱ, CK Shum^j, Bob E. Schutz^g, Benjamin Smith^h, Yuekui Yang^{a,k}, Jay Zwally^{a,c}

^a NASA Goddard Space Flight Center, Greenbelt, MD, United States

^b University of Colorado, Boulder, CO, United States

^c University of Maryland, College Park, MD, United States

^d University at Buffalo, Buffalo, NY, United States

^e Scripps Institution of Oceanography, La Jolla, CA, United States

^f Jet Propulsion Laboratory, California Institute of Technology, Pasadena, CA, United States

^g University of Texas, Austin, TX, United States

^h University of Washington, Seattle, WA, United States

ⁱ Texas A&M University, College Station, TX, United States

^j The Ohio State University, Columbus, OH, United States

^k Universities Space Research Association, Columbia, MD, United States

ARTICLE INFO

Article history:

Received 27 May 2016

Received in revised form 20 December 2016

Accepted 31 December 2016

Available online xxx

Keywords:

ICESat-2

Land ice

Sea ice

Vegetation

Climate change

Satellite mission

ABSTRACT

The Ice, Cloud, and land Elevation Satellite (ICESat) mission used laser altimetry measurements to determine changes in elevations of glaciers and ice sheets, as well as sea ice thickness distribution. These measurements have provided important information on the response of the cryosphere (Earth's frozen surfaces) to changes in atmosphere and ocean condition. ICESat operated from 2003 to 2009 and provided repeat altimetry measurements not only to the cryosphere scientific community but also to the ocean, terrestrial and atmospheric scientific communities. The conclusive assessment of significant ongoing rapid changes in the Earth's ice cover, in part supported by ICESat observations, has strengthened the need for sustained, high accuracy, repeat observations similar to what was provided by the ICESat mission. Following recommendations from the National Research Council for an ICESat follow-on mission, the ICESat-2 mission is now under development for planned launch in 2018. The primary scientific aims of the ICESat-2 mission are to continue measurements of sea ice freeboard and ice sheet elevation to determine their changes at scales from outlet glaciers to the entire ice sheet, and from 10s of meters to the entire polar oceans for sea ice freeboard. ICESat carried a single beam profiling laser altimeter that produced ~70 m diameter footprints on the surface of the Earth at ~150 m along-track intervals. In contrast, ICESat-2 will operate with three pairs of beams, each pair separated by about 3 km cross-track with a pair spacing of 90 m. Each of the beams will have a nominal 17 m diameter footprint with an along-track sampling interval of 0.7 m. The differences in the ICESat-2 measurement concept are a result of overcoming some limitations associated with the approach used in the ICESat mission. The beam pair configuration of ICESat-2 allows for the determination of local cross-track slope, a significant factor in measuring elevation change for the outlet glaciers surrounding the Greenland and Antarctica coasts. The multiple beam pairs also provide improved spatial coverage. The dense spatial sampling eliminates along-track measurement gaps, and the small footprint diameter is especially useful for sea surface height measurements in the often narrow leads needed for sea ice freeboard and ice thickness retrievals. The ICESat-2 instrumentation concept uses a low energy 532 nm (green) laser in conjunction with single-photon sensitive detectors to measure range. Combining ICESat-2 data with altimetry data collected since the start of the ICESat mission in 2003, such as Operation IceBridge and ESA's CryoSat-2, will yield a 15+ year record of changes in ice sheet elevation and sea ice thickness. ICESat-2 will also provide information of mountain glacier and ice cap elevations changes, land and vegetation heights, inland water elevations, sea surface heights, and cloud layering and optical thickness.

© 2016 Published by Elsevier Inc.

* Corresponding author.

E-mail address: Thorsten.Markus@nasa.gov (T. Markus).

1. Introduction

ICESat was the first spaceborne laser altimetry mission for Earth science and was in operation from 2003 to 2009 (Schutz et al., 2005). Because of laser lifetime issues, ICESat's collection strategy was changed from continual operation to 30 day campaign periods two to three times each year. Despite this campaign mode operation, it was a very successful mission that enabled estimates of the overall mass change of the Greenland and Antarctic ice sheets, as well as the regional changes that illuminate the underlying processes (Pritchard et al., 2009; Zwally et al., 2011 and 2015; Sørensen et al., 2011; Sasgen et al., 2012, Csatho et al., 2014, Khan et al., 2014).

One of the key findings of ICESat was that some outlet glaciers around the margins of these ice sheets are losing more mass quicker than expected (e.g., Pritchard et al., 2009; Zwally et al., 2011). Investigations using ICESat data resulted in the discovery and subsequent mapping of sub-glacial lakes in Antarctica (Fricker et al., 2007; Smith et al., 2009) and the improvement of tide models under ice shelves (Padman et al., 2008; Ray, 2008). ICESat altimeter data have been used to deconvolve ice and solid earth mass change signals for the Gravity Recovery and Climate Experiment (GRACE) data over Antarctic ice sheets (Gunter et al., 2009; Groh et al., 2012). Furthermore, ICESat observations provided a comprehensive assessment of ice shelf thinning in Antarctica and subsequent links to dynamic thinning of grounded tributaries (Pritchard et al., 2012).

Outside of the ice sheets, ICESat data played a critical role in resolving mass changes of mountain glaciers and ice caps (Moholdt et al., 2010; Gardner et al., 2011; Gardner et al., 2012; Moholdt et al., 2012) that were determined to have contributed one third of total sea level rise observed over ICESat's period of operation (Gardner et al., 2013). Glacier thickness changes from ICESat observations served as a basis to derive the first spatially resolved mass budget over the entire Hindu Kush–Karakoram–Himalaya region (Kääb et al., 2012), the peripheral glaciers, and ice caps of Greenland (Bolch et al., 2013).

ICESat also demonstrated that it is possible to extract sea ice freeboard, thickness, and volume from laser altimetry (e.g. Kwok et al., 2009; Farrell et al., 2009; Kurtz and Markus, 2012). Freeboard is the height of the snow or ice surface above the local sea surface. Sea ice thickness can be derived from freeboard by assuming local hydrostatic balance and with assumptions or estimates of sea ice and water densities as well as snow load on top the ice floes (see, for example, Kwok et al., 2009, Connor et al., 2013, Farrell et al., 2015).

Time series of inter-annual variation and mission-length trends in sea ice thickness for the entire Arctic and Southern Oceans could be calculated. Recent observations of Arctic sea ice coverage from satellite passive microwave data show that record or near-record lows in ice extents occurred in the years 2005–12. In September 2012, the summer ice extent reached another record minimum of 3.6×10^6 km² which was 2.2×10^6 km² or 30% less than the record set seven years earlier in September 2005. With this record, seasonal ice now covers more than half of the Arctic Ocean. Results from ICESat showed that over the 5 years (2004–2008) for which we have ICESat data the overall sea ice thickness of the Arctic Ocean multiyear ice decreased by 0.6 m, and >40% of the thick multiyear ice was lost (Kwok et al., 2009). Over decadal time scales, the combined record of submarine and ICESat thickness estimates suggest that winter thickness in the central Arctic has thinned from 3.64 m in 1980 to 1.75 m by 2009 (Rothrock et al., 2008; Kwok and Rothrock, 2009). Extending the ICESat time series with more recent observations from CryoSat-2 shows that ~ 1500 km³ of winter (February/March) sea-ice volume has been lost from the Arctic Ocean during the last decade between 2003 and 2012 (Laxon et al., 2013). As a result, there is a reversal in both the volumetric and areal contributions of the multiyear and seasonal ice to the total volume and area of the Arctic Ocean ice cover. While thinner, seasonal ice is common in the peripheral seas and ice margins, the Arctic ice cover

has clearly shifted to a regime where seasonal ice is now also prevalent in the interior of the Arctic Ocean. With a diminishing multiyear ice cover and thinner ice a significant fraction of the Arctic Ocean is now exposed to the atmosphere during the summer. For the coming decade, thickness estimates are needed for improved subseasonal-to-seasonal forecasts and refined projections of future climate patterns. ICESat also allowed for the first time a rough estimate of sea ice volume of the Antarctic sea ice cover (Kurtz and Markus, 2012).

Utilizing ICESat sea surface height measurements from leads across the Arctic sea ice pack, together with contemporaneous radar altimetry measurements from Envisat, Farrell et al. (2012) described the first mapping of the Arctic Ocean mean dynamic topography using satellite-only data. These sea surface height measurements were also used to derive a high-resolution, satellite-only marine gravity field model of the Arctic (McAdoo et al., 2013).

ICESat also enabled the estimation of global vegetation heights (e.g. Harding and Carabajal, 2005; Lefsky et al., 2007), global sea level anomaly and mesoscale variability features (Urban and Schutz, 2005), coastal ocean, ocean island and inland hydrology applications (e.g. Urban et al., 2008), as well as atmospheric characteristics (Spinhirne et al., 2005). Lefsky (2010), Simard (2011), and Los et al. (2012) generated global canopy height maps using ICESat in combination with other remote sensing data. Since ICESat digitized and recorded the full temporal profile of the received energy, additional research efforts were focused on analyzing specific waveform metrics to determine topographic characteristics and vegetation structure (e.g. Neuenschwander et al., 2008).

Despite ICESat's success the science community identified some limitations that prohibited the full exploitation of the dataset for scientific applications, particularly for determining change in the cryosphere. Therefore, different needs, requirements, and potential designs were discussed for an ICESat follow-on mission (Abdalati et al., 2010). It was concluded that to understand the governing processes that drive the large-scale changes in glacier and ice sheet elevation and sea ice thickness, changes in elevation should be monitored on a seasonal basis for the lifetime of the mission with improved spatial resolution beyond the observations provided by ICESat. Since the greatest elevation changes are known to occur at the glaciers along the margins of Greenland and Antarctica, there were added complications to the ICESat collection strategy in terms of deconvolving elevation change from surface slope and surface roughness. A single beam laser such as ICESat was not able to separate slope effects from true elevations changes on an orbit-by-orbit basis and thus many years of data were needed to separate these two effects (Howat et al., 2008; Pritchard et al., 2009; Moholdt et al., 2010). Improved spatial resolution and the ability to measure the cross-track slope were a critical consideration when developing the ICESat-2 mission. The multi-beam instrument design, smaller footprint, and the ability to resolve rougher terrains, would enable more accurate mountain and peripheral glacier mass balance measurements, allowing for improved quantification of land ice contributions to present-day sea level rise.

Similarly, a smaller footprint size, or rather higher spatial resolution, with increased spatial sampling intervals, will also enhance sea surface height and sea ice freeboard retrievals, and subsequently sea ice thickness calculations. While ICESat's campaign mode allowed the monitoring of inter-annual changes in sea ice thickness, monthly maps of sea ice thickness are needed to better understand freeze and melt processes as well as delineate dynamic versus thermodynamic sea ice thickening.

It was also determined that ICESat-2 should collect data over the mid- and lower-latitudes for land and ocean areas utilizing an operational off-nadir pointing capability in order to generate an optimized (non-repeat) collection of measurements for canopy heights that will contribute to the generation of a global carbon inventory assessment. Such an inventory is critical for understanding the global carbon budget.

To this end, the science objectives for ICESat-2 are defined as.

- Quantify polar ice-sheet contributions to current and recent sea-level change and the linkages to climate conditions;
- Quantify regional signatures of ice-sheet changes to assess mechanisms driving those changes and improve predictive ice sheet models; this includes quantifying the regional evolution of ice sheet change, such as how changes at outlet glacier termini propagate inward;
- Estimate sea-ice thickness to examine ice/ocean/atmosphere exchanges of energy, mass and moisture;
- Measure vegetation canopy height as a basis for estimating large-scale biomass and biomass change.

This paper explains how these science objectives translate into science requirements and subsequently into the measurement concept and implementation of the ICESat-2 mission.

Other areas of Earth science will also benefit from the ICESat-2 mission. The atmospheric community will have access to derived atmospheric and cloud properties while the oceanography community will be given global ocean and wave heights. The hydrological community will be provided global inland water body height and associated properties (Jasinski et al., 2016), as well as terrestrial snow thickness and permafrost monitoring.

2. Science requirements

Based on the mission objectives established by the ICESat-2 Project together with the ICESat-2 Science Definition Team the following Baseline Science Requirements were developed. These Baseline Science Requirements drive the mission design and the formal requirements flow-down to the spacecraft, instrument, and ground system component levels. In addition, Threshold Requirements are defined that represent the minimum requirements that need to be met for the mission to be considered successful in case trade-offs are necessary because of underperforming components.

a) ICESat-2 shall produce an ice surface elevation product that enables determination of ice-sheet elevation change rates to an accuracy of better than or equal to 0.4 cm/yr on an annual basis.

For the Threshold Requirement the required accuracy is 2 cm/yr.

This high accuracy can be achieved because of the many independent measurements over each of the ice sheets. The value of 0.4 cm/yr for the entire areas of the Greenland and Antarctic ice sheets corresponds to mass changes of 51 Gt/yr for Antarctica and 6 Gt/yr for Greenland assuming that all changes occur due to changes in ice thickness with a density of 917 kg/m³. For Antarctica, this corresponds to about 85% of the current mass loss (assuming an average of – 60 Gt/yr; Shepherd et al., 2012) and to 2.5% of Greenland's mass loss (assuming an average of – 240 Gt/yr; Shepherd et al., 2012). While the fraction for Antarctica seems large, Antarctica mass balance estimates range from + 100 Gt/yr to about – 200 Gt/yr (Shepherd et al., 2012). An accuracy of 51 Gt/yr is about 1/6 of the current mass balance uncertainty. An accuracy of 57 Gt/yr in ice mass balance for the two ice sheets combined corresponds to 0.15 mm in sea level change, which is about ~5% of the current rate (Hay et al., 2015) and ~20% of the error.

b) ICESat-2 shall produce an ice surface elevation product that enables determination of annual surface elevation change rates on outlet glaciers to an accuracy of better than or equal to 0.25 m/yr over areas of 100 km² for year-to-year averages.

For the Threshold Requirement the required accuracy is 0.5 m/yr.

Change detection to 0.25 m/yr will enable the detection of dynamically-significant changes in outlet glaciers. For most Greenland outlet glaciers, the rate of surface elevation change is on the order of a few meters to tens of meters per year, with progressively smaller changes farther upstream (Pritchard et al., 2009; Thomas et al., 2009). Typical Greenland outlet glaciers are on the order of 2–5 km wide and 20–50 km long, so 100 km² is a typical area scale for the fast-changing parts of the ice sheet. Measuring elevation changes to 0.25 m/yr will enable the determination of the magnitude of outlet glacier changes, and

will allow the monitoring of the extent to which changes in the outlet glaciers are driving smaller changes, over larger areas, in the inland ice sheet. Understanding the inland extent of elevation changes driven by the outlet glaciers is critical for understanding the potential future contributions of Greenland and Antarctica to sea level rise (Price et al., 2011).

In Antarctica, where elevation change rates are smaller, greater accuracy is required. However outlet glaciers are generally larger in Antarctica, and the expectation is that the characteristics of the measurement error (e.g., correlation lengths) will be such that measurements will have sufficient accuracy for most large Antarctic outlet glaciers.

c) ICESat-2 shall produce an ice surface elevation product that enables determination of surface elevation change rates for dynamic ice features that are intersected by its set of repeated ground-tracks to an accuracy of better than or equal to 0.4 m/yr along 1-km track segments.

For the Threshold Requirement the required accuracy is 0.8 m/yr.

One of the biggest unexpected discoveries of ICESat was the number, size, and dynamics of subglacial lakes located under the Antarctic ice sheet. (Smith et al., 2009, Fricker et al., 2007). Analysis of repeated ICESat tracks showed unexpected large elevation changes over many areas of the assumed stable inland Antarctic ice sheet. Similarly, ICESat repeat-track data have also been useful in measuring grounding-line positions based on short-scale pass-to-pass surface changes. (Fricker et al., 2009, Brunt et al., 2010, Brunt et al., 2011). The exact repeat-track orbit of ICESat enabled these studies of small-scale elevation changes and similar repeat tracks for ICESat-2 will enable the continuation of both of these types of studies, and, over the course of the mission, will allow estimates of grounding-line change for Antarctic ice shelves and Greenland outlet glaciers.

d) ICESat-2 shall produce an ice surface elevation product that enables resolution of winter (accumulation) and summer (ablation) ice-sheet elevation change to 10 cm at 25-km × 25-km spatial scales.

For the Threshold Requirement the required accuracy is 5 cm but is limited to areas with a slope of <1° (essentially excluding outlet glaciers).

This accuracy represents approximately 10% of the seasonal amplitude of ice surface elevation change for coastal Greenland. Measuring seasonal elevation changes offers multiple benefits to cryospheric studies: It allows calibration of atmospheric models estimating accumulation and ablation from the ice sheets (Ligtenberg et al., 2012) and validation of firn densification models (Kuipers Munneke et al., 2015). It also provides mass change time series comparable in accuracy and temporal resolution to gravimetric estimates of ice-sheet change (i.e. from GRACE), and it will allow the subtraction of the surface-mass-balance-driven elevation change from outlet-glacier elevation changes, isolating the dynamic signal (Csatho et al., 2014).

e) ICESat-2 shall provide monthly surface elevation products to enable, when sea surface height references (leads) are available and under clear sky conditions, the determination of sea-ice freeboard to an uncertainty of less than or equal to 3 cm along 25-km segments for the Arctic and Southern Oceans; the track spacing should be less than or equal to 35 km at 70° latitude on a monthly basis.

The Threshold Requirement retains the 3 cm freeboard uncertainty but relaxes the length scale to 50 km.

Deriving sea ice freeboard and subsequently sea ice thickness and changes in thickness requires the ability to discriminate the sea surface height from surrounding sea ice height for freeboard determination. Since only a small fraction (roughly 1/10) of the floating sea ice is above the water level, small errors in freeboard retrieval can result in large errors in the scaling of freeboard to estimates of sea ice thickness. The required 0.03 m height measurement precision corresponds to an accuracy of ~0.3 m in thickness or an overall uncertainty of <25% of the current annual ice-volume production of the Arctic Ocean. Measurement at this level will enable accurate determination of the spatial

ranges of mean ice thickness of 2 to 3 m across the Arctic and Southern Oceans. Furthermore, monthly data sampling of the ice-covered Arctic and Southern Oceans is required to resolve the seasonal cycles in ice growth and decay. Monthly averages are the longest temporal scale that can be used to create coherent sea ice thickness maps without significant interference of the seasonal cycle. ICESat-2's dense along-track sampling, and multi-beam configuration, will also provide detailed knowledge of sea ice surface characteristics and morphology.

f) ICESat-2 shall make measurements that span a minimum of three years.

The Threshold Requirement retains the three year operation requirement but allows the mission to only take science data for 182 day per year providing at least seasonal sampling.

The mass evolution of the ice sheets exhibits significant seasonal and inter-annual variations as observed by satellite gravimetry (Luthcke et al., 2013). Fig. 1 presents the mass evolution of the Greenland ice sheet from a recent NASA GSFC GRACE mascon solution (update to Luthcke et al., 2013). The time series exhibits significant inter-annual variation including the extreme 2012 summer mass loss followed by a pause in mass loss. A minimum of 3 years of ICESat-2 observations are necessary to fully observe the seasonal and inter-annual variations in order to compute the mass balance from ICESat-2, the decadal ICESat and ICESat-2 inter-mission mass balance, and to facilitate comparison and combination with GRACE and GRACE-Follow-On (<http://gracefo.jpl.nasa.gov>) data for a multi-decadal mapping of ice sheet change.

The Threshold Requirement allows, if necessary, to operate ICESat-2 in a campaign mode similar to ICESat in order to increase mission lifetime, but still capture the extremes and inter-annual variations of the seasonal cycle.

g) ICESat-2 shall produce an ice surface elevation product that, in conjunction with ICESat, enables determination of elevation changes on a decadal time scale.

This requirement is unchanged for the Threshold Requirements.

The detailed Greenland Ice Sheet laser altimetry record (1993–2012) using both airborne and satellite data shows large spatial and temporal variations of dynamic mass loss and widespread intermittent thinning with rapid thinning periods lasting from a few years to >15 years (Csatho et al., 2014). This complexity of ice sheet response to climate forcing points to the need for decadal or longer monitoring of the ice sheets at high spatial resolution. Careful monitoring of measurement biases, trends, and errors is needed for the establishment of a long time series.

h) ICESat-2 shall produce elevation measurements, that enable independent determination of global vegetation height, with a ground track spacing of <2 km over a 2-year period.

This requirement is deleted in the Threshold Requirements.

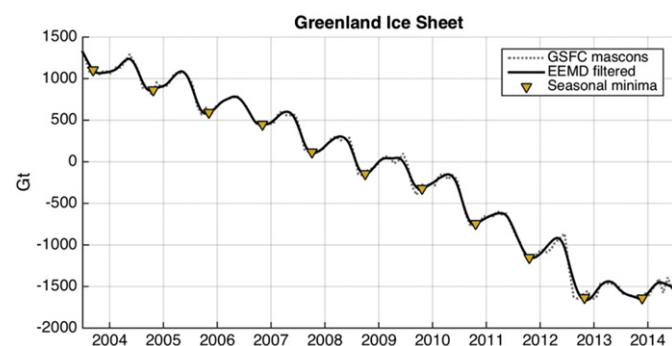


Fig. 1. Greenland ice sheet cumulative mass change time series from NASA GSFC mascon solution (update to Luthcke et al., 2013). Mascon solution shown as dashed line with Ensemble Empirical Mode Decomposition (EEMD) filtered mascon solution time series as solid line with seasonal minima determined from EEMD analysis (Loomis and Luthcke, 2014). Significant inter-annual variations are observed including the extreme summer mass loss in 2012 followed by the recent pause in mass loss.

Forests play a significant role in the terrestrial carbon cycle as carbon pools. Events, such as management activities (Krankina et al., 2012) and disturbances can release carbon stored in forest above ground biomass into the atmosphere as carbon dioxide, a greenhouse gas that contributes to climate change (Ahmed et al., 2013). While carbon stocks in nations with continuous national forest inventories (NFIs) are known, complications with NFI carbon stock estimates exist, including: (1) ground-based inventory measurements are time consuming, expensive, and difficult to collect at large-scales (Houghton, 2005; Ahmed et al., 2013); (2) asynchronously collected data; (3) extended time between repeat measurements (Houghton, 2005); and (4) the lack of information on the spatial distribution of forest above ground biomass, required for monitoring sources and sinks of carbon (Houghton, 2005).

Based on the global carbon budget for 2015 (Le Quéré et al., 2015), the largest remaining uncertainties about the Earth's carbon budget are in its terrestrial components, the global residual terrestrial carbon sink, estimated at 3.0 ± 0.8 GtC/year for the last decade (2005–2014). Similarly, carbon emissions from land-use changes, including deforestation, afforestation, logging, forest degradation and shifting cultivation are estimated at 0.9 ± 0.5 GtC/year. By providing information on vegetation canopy height globally with a higher spatial resolution than previously afforded by other spaceborne sensors, the ICESat-2 mission can contribute significantly to reducing uncertainties associated with forest vegetation carbon.

It is anticipated that the data products for vegetation will be complementary to ongoing biomass and vegetation mapping efforts. Synergistic use of ICESat-2 data with other space-based mapping systems (e.g. the Global Ecosystem Dynamics Investigation Lidar (GEDI); <https://science.nasa.gov/missions/gedi/>) or imaging sensors, such as optical or radar (e.g. the NASA-ISRO SAR Mission (NISAR); <http://nisar.jpl.nasa.gov>), is one solution for extended use of ICESat-2 data.

i) The ICESat-2 Project shall conduct a calibration and validation program to verify delivered data meet the requirements a, b, c, d, e, g and h.

This requirement is unchanged for the Threshold Requirements.

Calibration and validation of the ICESat-2 products is a critical component of the mission. Rigorous effort is required during pre-launch studies as the instrumentation is characterized and relevant models are developed to support an accurate understanding of the operational aspects of the instrument as environmental and mechanical parameters vary. Additionally, a comprehensive calibration and validation plan will be initiated once ICESat-2 is on orbit in order to establish an accurate understanding of all of the ICESat-2 data products in terms of uncertainties and potential biases. This effort will establish confidence in the scientific data and verify that the requirements of the mission have been achieved. This requirement is obvious because without calibration and validation and without rigorous uncertainty and error assessment any geophysical products would remain questionable.

3. Measurement and mission concept

The baseline requirements above drive the top-level mission design, its implementation, and operations plan. The ICESat-2 mission carries a single instrument, the Advanced Topographic Laser Altimeter System (ATLAS). This section is divided into descriptions of the required sampling geometry, elevation precision, bias monitoring, geophysical corrections, and coverage. All are critical aspects considered when developing ICESat-2 and ATLAS technical capabilities.

The measurement concept of the ICESat-2 instrument is quite different from an analog laser altimeter like onboard ICESat. The ICESat-2 micropulse laser will produce much less energy per pulse but with a 10 kHz repetition rate. This increased repetition rate will result in a 0.7 m separation for each laser pulse on the surface. This is ideal for rough and heterogeneous terrain such as glaciers or sea surface heights where the minimal gaps in along-track measurements will provide a higher fidelity of the topography. The inherent detection requirement

associated with the lower power of the micropulse laser is detector sensitivities on the single photon level. This requirement is achieved through the use of photomultiplier tubes (PMTs) as detectors where single photons reflected from the surface will trigger a detection within the ICESat-2 receiver. Each individual photon will be time tagged and geolocated. This scenario is much different than the full-waveform data collected by ICESat for each laser footprint.

3.1. Sampling geometry

ICESat-2 will have a total of 6 beams organized in a 2×3 array. By slightly yawing the spacecraft during flight this will create three pairs of beams on the ground with each pair being separated by 3.3 km and a pair width of 90 m (see Fig. 2). The pair width is adjustable on orbit by changing the yaw angle.

To achieve high spatial resolution and discriminate elevation change from cross-track surface slope, closely separated pairs of beams are required. This is a critical capability needed to meet the science requirements associated with the ice sheets in particular. Fig. 3 depicts the differences in the collection strategy of ICESat and ICESat-2 where the multi-beam configuration supports annual and seasonal elevation change determination independent of cross-track surface slope.

The location of the laser spot will not perfectly follow the reference ground tracks (RGT) for repeated measurements due to limitations in pointing control. The actual laser spots may be a slightly offset (the orange and green lines in Fig. 3) from the RGT (black lines in Fig. 3). To meet the science objectives and ice sheet science requirements, ICESat-2 will utilize pairs of beams (Fig. 3, right side). The concept is that each time the satellite passes over the RGT one beam is to the left and one to the right of the RGT. This makes it possible to calculate the local cross-track slope and interpolate the elevation to the RGT. Because cross-track surface slope is not known a-priori it is ambiguous whether

the elevation derived from subsequent passes is real change or whether the measured elevation differences are a result of track location differences over a sloped surface. For ICESat several years of data were required to extract the surface slope (assuming the slope did not change over that time period) before the elevation change could be determined (e.g. Howat et al., 2008; Pritchard et al., 2009; Smith et al., 2009; Moholdt et al., 2010). Multiple beam pairs will mitigate the uncertainties associated with the assumptions of surface slope characteristics ensued from ICESat single beam collection configuration.

A pair-spacing requirement of 90 m is based on a sampling analysis of airborne laser-altimetry data collected with the Airborne Topographic Mapper (ATM) over Russell Glacier, in Southwest Greenland, which spans a wide range of surface roughnesses (Fig. 4, top). In this analysis, the collection of point elevation measurements was sampled using different potential beam spacings and random repeat-track geometries, and the RMS error calculated in the resulting surface-change measurements. Fig. 4, bottom, shows the elevation-difference accuracy as a function of surface roughness for different beam spacings. For all roughness values, the error increases with the pair spacing, but for the small (<0.5 m) roughnesses typical of the interior of the ice sheet, the ICESat-2 error is small for spacings <100 m, increasing sharply for larger spacings. This reflects the lack of significant surface topography at scales smaller than about 100–200 m over uncrevassed ice, which lets repeat track sampling at scales finer than 100 m correct for the shape of the surface topography, while at larger spacings, the fine-scale topography is undersampled and leads to an elevation-change error. To interpolate to the RGT, ICESat-2 needs to control the beam position to less than half the pair separation. Thus a pointing control ≤ 45 m is required.

One component of the elevation error over areas with surface slope is directly related to geolocation knowledge derived in post-processing multiplied by the tangent of the slope. The requirement for pointing knowledge after post-processing is 6.5 m, which translates into an

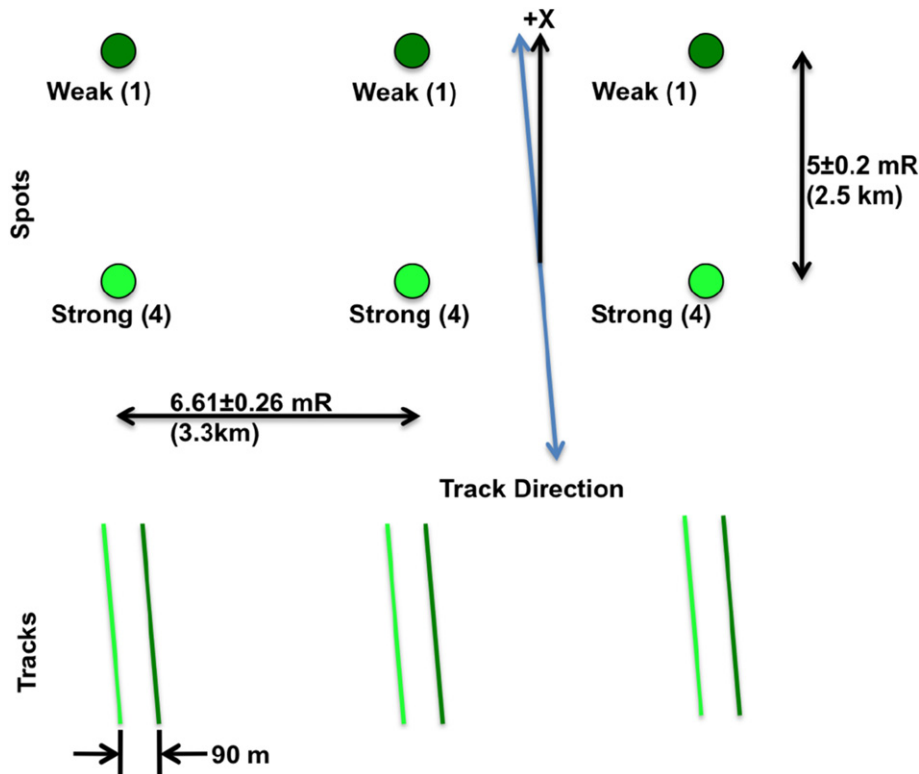


Fig. 2. ICESat-2's sampling geometry. The beam pattern is a 3×2 array that, by slightly yawing the spacecraft, creates three pairs of beams on the ground. The planned separation for each pair is 90 m but this can be changed on orbit by changing the yaw angle.

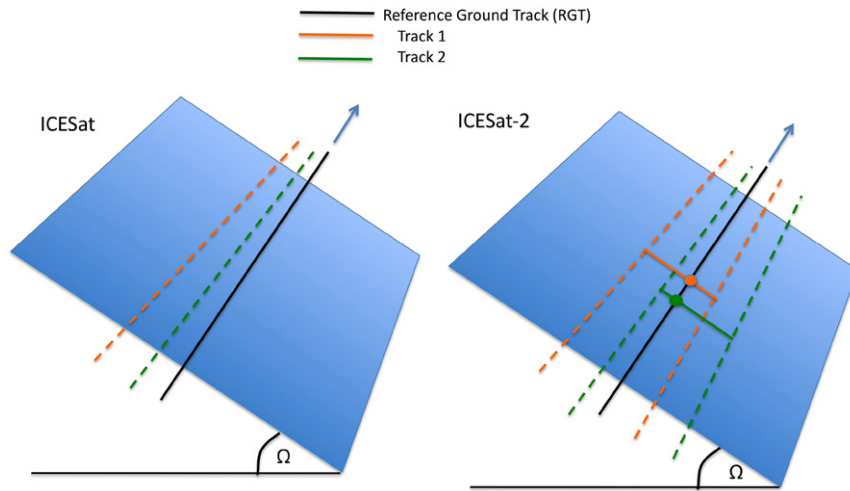


Fig. 3. Comparison of elevation change retrievals from ICESat and ICESat-2. With an unknown slope Ω and near coincident tracks it is impossible to calculate elevation change from two single-beam tracks (ICESat; left). ICESat-2 (right) has pairs of beams that straddle the reference ground track so that its elevation can be extracted through interpolation of the elevations measured by the two beams.

elevation error of about 0.5 m over slopes with 5° , a typical slope of the glaciers along the coasts of the Greenland and Antarctic ice sheets. For most of the ice sheets the slope is much smaller (Fig. 5). Fig. 5 shows the surface slope magnitude and roughness calculated from ICESat elevation data, masked using information from a visible-imagery mosaic of Antarctica (Haran et al., 2005) to include only ice-sheet surfaces. These data cover the ice sheet to a latitude of 86° , and accurately resolve variations in surface slope at horizontal scales as small as 170 m. Slopes are small ($<0.5^\circ$) except near coasts and where glaciers flow through mountains. Surface roughness is also small (<0.25 m) except in coastal areas, in crevassed shear margins, and in a few parts of the ice-sheet interior where wind erosion produces meter-scale surface features.

ICESat-2's orbit will have an inclination of 92° enabling measurements up to 88° north and south, with a 91-day exact repeat cycle. This will ensure seasonal repeat tracks that are needed for the seasonal ice sheet requirement (Requirement d). Because, as stated in Requirement e), Arctic- and Southern Ocean-wide sea ice freeboard maps shall be generated on a monthly basis an orbit was chosen with a near-monthly sub-cycle resulting in an even distribution of tracks every month. Since ICESat took measurements in 30-day campaign modes, the actual increase in coverage compared to ICESat is nine times over a 91-day period.

3.2. Elevation precision

Individually timed and geolocated photons do not in themselves provide direct information of the elevation of the surface because a priori the source of any given photon is unknown. It may have originated from reflection of a laser pulse off a cloud or sunlight of the same wavelength may have scattered back into the telescope. Photons from several shots need to be accumulated and statistically analyzed. Statistically the density of photons reflected from the surface is much greater than the more evenly distributed photons from the atmospheric column so that the elevation of the earth surface can be determined using statistical characteristics and noise filtering. The actual elevation precision depends on the signal-to-noise ratio, on the length or distance over which laser shots are accumulated, and the precision with which each photon can be timed. Model calculations were used to predict ICESat-2's radiometric performance over various surfaces and the results guided requirements flowdown and instrument design. Not all beams have the same energy to keep the required laser energy low and because cross-track slope retrieval is only needed for the highly reflective ice

sheets where the number of signal photons is high. Therefore, each beam pair consists of a strong and a weak beam. The strong beam has four times the energy of the weak beam and consequently four times the number of returned laser photons per shot.

Table 1 shows the predicted number of return photons received per shot for different surface types and also the standard deviations of range for 100 shot accumulations, which is equal to 70 m along track. Return strength in photoelectrons per shot was calculated using the transmitted energy, the instrument optical throughput and detector efficiency, and atmospheric and surface reflectance parameters that define each design case. The temporal distribution of return photoelectrons was modeled using a transmitted pulse profile and receiver impulse response, and surface impulse responses derived from the surface parameters such as slope, roughness and type (ice or water) that define each design case. The number of detection events per shot was calculated using the number and distribution of photoelectrons and a model of the PMT's deadtime behavior. The range in the number of expected return photons and standard deviations for each surface type is a function of the environmental conditions such as surface roughness and reflectance. For high-reflectivity targets, such as ice sheets, the weak beams returns a sufficient number of laser photons to enable elevation measurements.

To enable the development of retrieval algorithms, an ICESat-2 airborne simulator, the Multiple Beam Experimental Lidar (MABEL) (McGill et al., 2013), was flown over sea ice (Kwok et al., 2009; Farrell et al., 2015), ice sheets (Brunt et al., 2014; Brunt et al., 2016), vegetated areas (Herzfeld et al., 2014; Gwenzl and Lefsky, 2014; Glenn et al., 2016), cities, oceans, and lakes (Jasinski et al., 2016) during different seasons. MABEL's pulse repetition rate is variable (5 to 25 kHz) and was 5 kHz for the data presented here. At the nominal altitude of ~ 20 km and at an aircraft speed of ~ 200 m s^{-1} , MABEL samples a ~ 2 m footprint every ~ 0.04 m along-track. More specifications on MABEL are given in Appendix A. The spacing between the individual beams was configured to allow simulation of the planned beam geometry of ATLAS. Owing to non-uniform optical paths (fiber lengths) through the instrument, the transmit-pulse energies are generally not equal. Consequently, the number of signal photons per shot was also not equal. They furthermore differed between the different campaigns.

Descriptions of the campaigns as well as the data are available via <http://icesat-2.gsfc.nasa.gov/data>. The data collections were planned to provide the critical sample data needed in the development of the ICESat-2 algorithms by varying surface type and season of acquisition.

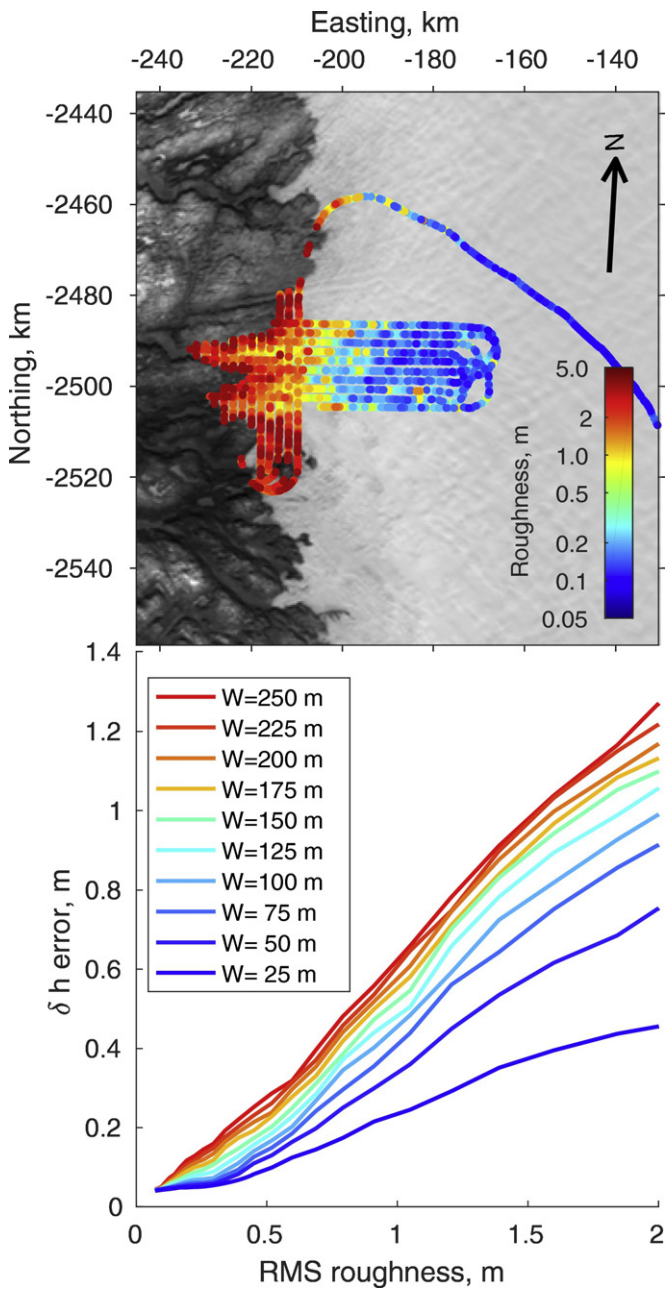


Fig. 4. Top: surface roughness, calculated as the RMS difference between elevation measurements and 200-m linear segments, measured over lower Russell Glacier, Southwest Greenland. The scale is about 100 km horizontal and vertical. Northing and Easting give coordinates in a polar stereographic projection with a true-scale at 70 N and a central meridian of -45 E. Bottom: Height-recovery errors as a function of beam spacing (W) and surface roughness for simulated ICESat-2 data. Roughness values <0.5 m are typical of inland ice while larger values reflect surface crevassing.

The altitude of many of these flights was about 20 km (65,000 ft) above sea level so that 95% of the atmospheric contribution was between the instrument and the Earth’s surface. This facilitates the development of algorithms for atmospheric properties and also provides realistic atmospheric photon distributions that may impact the ground finding algorithms. Fig. 6 shows some examples from these flights for three surface types.

The data show the time-tagged photon elevations as a function of distance along-track (Fig. 6, left panel). While there appear to be a significant number of solar photons in all three examples, the number of

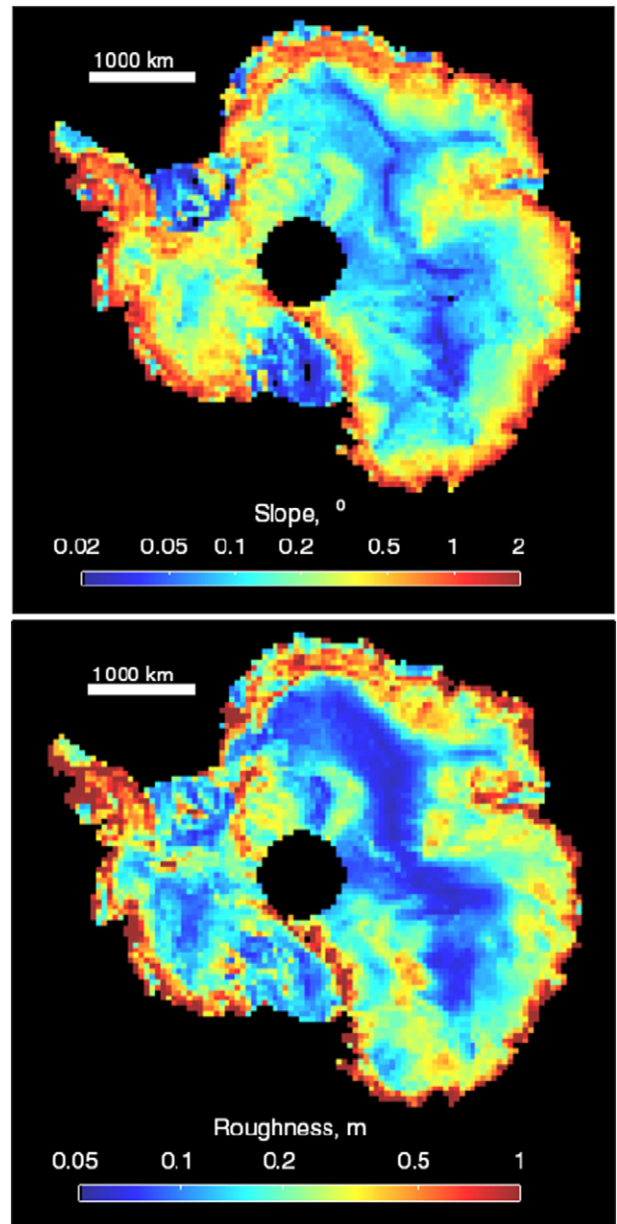


Fig. 5. Top: Ice sheet surface slope magnitude for the entire continent of Antarctica, calculated as the 68th percentile of surface slopes for 50×50 km squares on the ice-sheet surface. Data are in a polar stereographic projection with a true-scale at 70 S. The south pole is in the center of the figure with 0E straight up. Bottom, ice sheet roughness calculated as the 68th percentile of the absolute difference between each measured elevation and the average of its two nearest along-track neighbors, for the same grid used for the slope map.

photons reflected from the surface is much greater and densely clustered compared to the more evenly distributed photons from either the atmosphere or solar background so that the elevation of the earth surface and also its properties can be extracted. The number of solar photons is primarily a function of the surface reflectivity and the solar angle. As shown in Fig. 7, for a Lambertian surface, the highest clear sky solar background rate is about 14.5 MHz (for overhead sun), but since most of the high albedo areas are in the polar regions, where the solar zenith angles are generally large, high background rates of solar photons are about 10 MHz, which translates to two solar photon every ~ 60 m vertically. At night these photons will be minimal. The detectors themselves also are subject to some noise but measurements have shown that the detector dark count rate is 1000 Hz and thus negligible. The quantitative estimate of surface elevation and canopy

Table 1
ATLAS expected performance in range using the current best estimates for winter and summer conditions.

Target type	Lambertian surface reflectance (532 nm)	N signal photons per shot (weak beam)	N signal photons per shot (strong beam)	100-shot std. dev (weak beam) [cm]	100-shot std. dev (strong beam) [cm]
Ice sheet (interior)	0.9–0.98	0.4–3.0	1.6–12.0	4–9	2–4
Ice sheet (glaciers)	0.6–0.9	0.6–1.0	0.6–3.9	12–29	6–14
Sea ice	0.8–0.9	0.6–2.1	2.3–8.5	5–8	3–4
Leads	0.1–0.2 (much higher when specular)	0.05–0.2	0.2–1.0	2–5	2–5

heights is done by the generation of histograms (Fig. 6, right panel) of photon densities and statistical analyses. This is an active area of research as algorithms are being developed primarily using MABEL data (Kwok et al., 2014; Farrell et al., 2015; Brunt et al., 2014; Brunt et al., 2016; Herzfeld et al., 2014; Gwenzi and Lefsky, 2014; Glenn et al., 2016; Jasinski et al., 2016).

The top row of Fig. 6 shows an example of the interior Greenland ice sheet. For these relatively flat areas, the 200 m histogram has a very clear peak above the noise, enabling the identification of surface elevation. Fig. 6 also indicates that for smooth high-reflectivity areas, histograms over much shorter distances will be sufficient to extract surface elevation with high confidence, increasing the along-track spatial resolution of elevation retrievals. Because each received photon is timed and geolocated, the length over which photons are accumulated for the calculation of surface elevation is flexible and can be optimized in algorithms depending on accuracy and precision requirements.

For sea ice (Fig. 6, middle plots), there is an elevation difference between the flat leads and the rougher and higher sea ice. To estimate the freeboard, elevations of both the sea ice and the open water need to be calculated. The red vertical lines for sea ice and green vertical lines for the open water indicate example areas. The corresponding histograms have peaks at different elevations, which directly correspond to the sea ice freeboard. Kwok et al. (2009) and Farrell et al. (2015) provide a detailed discussion of the identification of leads using MABEL data for the retrieval of sea surface heights and the derivation of freeboard and thickness.

Fig. 6 (bottom) shows an example of MABEL returns over vegetation. The histogram of photons between the red lines shows two distinct peaks. The upper, broader, peak is from photons reflected off the tree crowns whereas the lower, sharper peak is from the ground surface below the trees. Analysis of histograms or photon densities will allow the retrieval of tree heights and potentially also yield information of tree structure or type (Glenn et al., 2016). The strength of the ground surface signal is a function of canopy density.

In addition to surface products, ICESat-2 will also collect data for the entire lower atmosphere. While every photon around the surface will be timed and geolocated to preserve full resolution and highest elevation accuracy, data over the atmospheric column are accumulated 30 m vertically and 280 m along-track onboard the spacecraft to reduce data volume. Fig. 8 shows a plot of photon densities collected by the MABEL instrument. Areas of higher densities can be attributed to different types of clouds. The flat line of high photon densities at the bottom of Fig. 8 is from surface returns. When the cloud optical depth becomes too high the surface signal is lost.

3.3. Bias monitoring

Most ICESat-2 requirements are expressed in elevation change. It is therefore imperative to monitor changes in the instrument bias that may be expressed as range or elevation change. Several measures are taken to ensure that instrument changes are monitored and accounted for in post-processing. The mission has a requirement to monitor changes in elevation bias to 0.2 cm per year over the full life of the mission and to provide long-term trend analyses of observatory performance. Pre-launch, the instrument team will characterize the change in range bias as a function of telemetered temperatures. On orbit, the instrument

will monitor and calibrate changes in range bias using Transmit Echo Calibration. The Transmitter Echo is a small sample of the transmitted pulse, carried directly to the receiver by fiber optics. Monitoring its measured time of flight will indicate any changes in the receiver's timing bias. This will be done for two beams and the results can be compared to the pre-launch data. In post-processing data analysis, range bias changes for the other four beams will be examined by comparing short-period (<24 h) crossovers (in 10-day groups) of the calibrated with the un-calibrated beams.

Analysis of altimetry data during ocean scan maneuvers will be used to calibrate pointing and separate these errors from ranging errors (Luthcke et al., 2000; Luthcke et al., 2005). Ocean scans are routine calibration activities where the instrument will be pointed off-nadir by $\leq 5^\circ$ and perform conical scans. The expected range bias error is determined from a high fidelity simulation where 10-days of altimeter range crossover data are simulated between all known and unknown beams including altimeter range observation, orbit and attitude error. The crossovers are then edited to include only cross-overs with <1-day of time separation between crossing tracks in order to minimize correlation with geophysical signal. The 1-day binned cross-overs residuals are then reduced formally estimating the range biases for the unknown beams. One hundred simulations are run, each with a new realization of the errors. Fig. 9 shows the standard deviation of the difference between the true range biases and the estimated range biases over the 100 simulations as a function of latitude. The range bias error is significantly smaller at high latitudes due to the increased number of crossover observations moving to high latitudes. These simulations suggest a <5 mm range bias calibration error every 10 days for the ice sheets. The long-term drift would be <1 mm/year.

3.4. Geophysical corrections

The primary measurement of the mission is the photon time of flight from the satellite to the Earth's surface and back, but most science applications require converting range into height with respect to a reference ellipsoid. Hence, the science-directed data products require systematic removal of various geophysical signals to enhance their scientific usability. Various present-day models of ocean tides, earth tides, pole tides, dynamic ocean response, and ocean loading, among other geophysical phenomena are used to determine these geophysical corrections.

A set of corrections will be applied to the ICESat-2 ATL03 data product (which provides latitude, longitude, and height for each recorded photon event). A design criterion is that these corrections be easily removable for investigations involving improvements to the corrections themselves or for cases when an investigator desires that a different model be applied.

Ocean tides: Incorporating the assessment by Stammer et al. (2014), ICESat-2 has adopted the GOT4.8 ocean tide model of R. Ray (NASA/GSFC). Over open oceans, ocean tides have typical amplitudes of ± 80 cm, but tides be as large as several meters in coastal and estuary regions as well as under ice shelves.

Ocean tidal loading: ICESat-2 has adopted loading harmonic grids from the GOT4.8 tide model of R. Ray (NASA/GSFC) and include 9 major and 16 minor tidal constituents. Over open oceans, ocean tidal loading amplitudes are on the order of 5% of the ocean tide. This correction ranges from -6 to 0 cm.

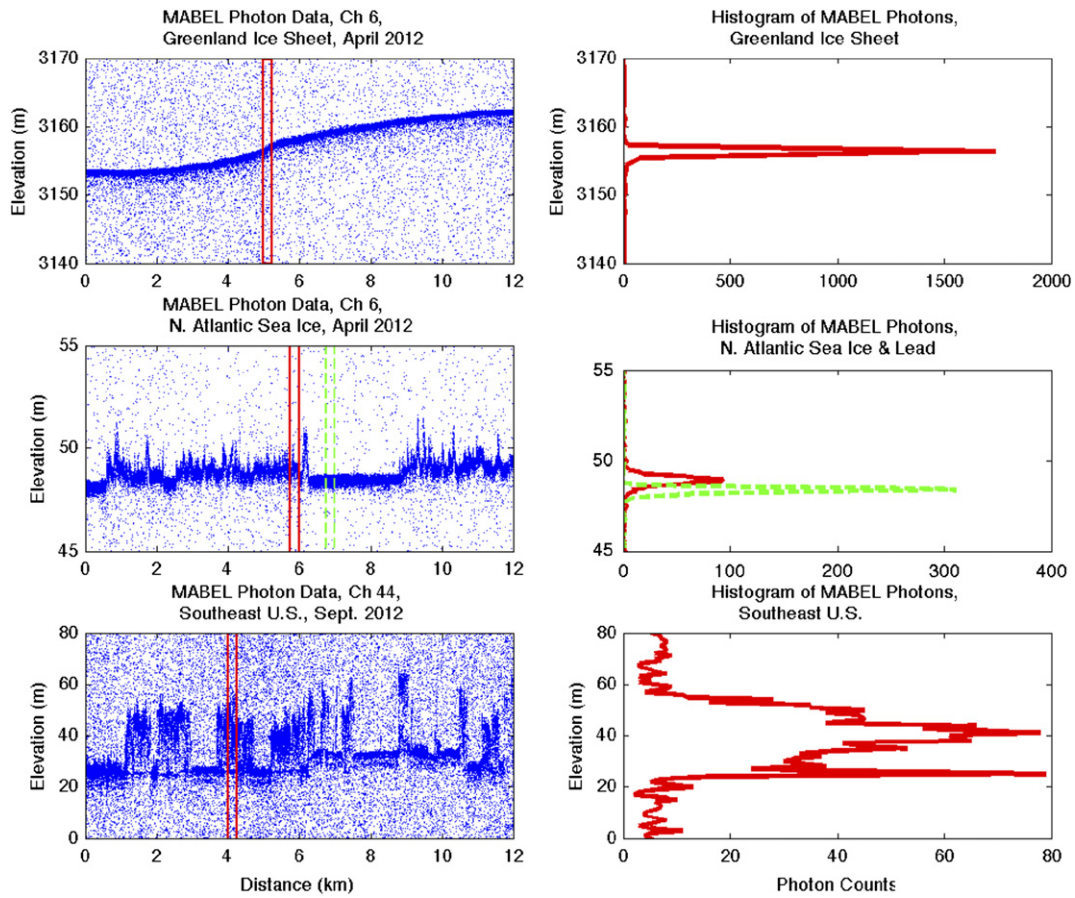


Fig. 6. Typical ICESat-2-like data from MABEL over the Greenland ice sheet (top), sea ice (middle), and vegetated land surface (bottom). The histograms on the right show photon distributions for the areas between the two red and green vertical lines in the photon clouds. The distance between the lines is 200 m for these examples. In the actual algorithms that are currently being developed for operational processing this distance will be optimized and may vary as a function of signal-to-noise ratio, surface roughness, and number of signal photons. (For interpretation of the references to color in this figure legend, the reader is referred to the web version of this article.)

Solid earth tides: ICESat-2 has adopted the International Earth Rotation and Reference System (IERS) 2010 convention for solid earth tides to take into account the deformation (elastic response) of the solid earth (including the sea floor) due to the attractions of the Sun and Moon. These are applicable globally, and have amplitudes typically on the order of ± 40 cm.

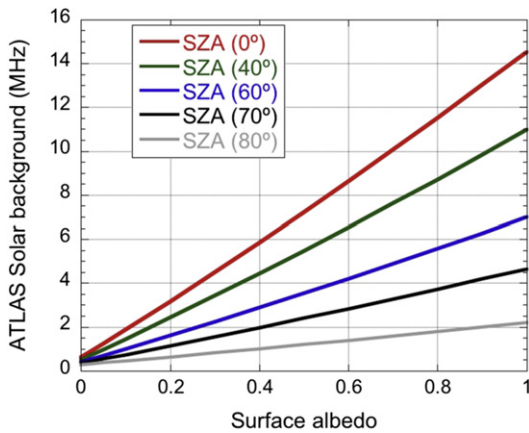


Fig. 7. ATLAS clear sky solar photon rate as a function of surface albedo for different Solar Zenith Angles (SZA). Surface is assumed Lambertian. Simulations done with the Discrete Ordinates Radiative Transfer model (DISORT) (Stamnes et al., 1988). ATLAS parameters used in the calculations include: telescope diameter (0.8 m), field of view (85 μ rad), detector quantum efficiency (0.15), total receiver transmission (0.504) and filter width (0.038 nm).

Dynamic atmospheric correction and inverted barometer effect: ICESat-2 has adopted the utilization of global, empirical, 6-h, AVISO MOG2D, $1/4^\circ \times 1/4^\circ$ grids to be used as a near-real-time Inverted Barometer (IB) and Dynamic Atmospheric Correction (DAC, Carrère & Lyard, 2003). These grids are forced by the European Center for Medium-Range Weather Forecasting (ECMWF) model for the surface pressure and 10 m wind fields. This combined correction typically has amplitude on the order of ± 50 cm.

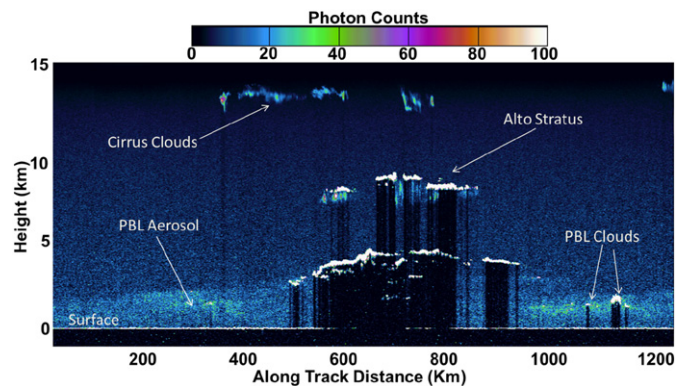


Fig. 8. Photon densities for a 15 km range in altitude and horizontal distance of about 100 km; the brighter the colour the higher the photon density. In addition to the surface different types of clouds (PBL stands for “planetary boundary layer”) can be identified. Data were taken with the MABEL instrument on September 21, 2013 over the southern portion of the Chesapeake Bay.

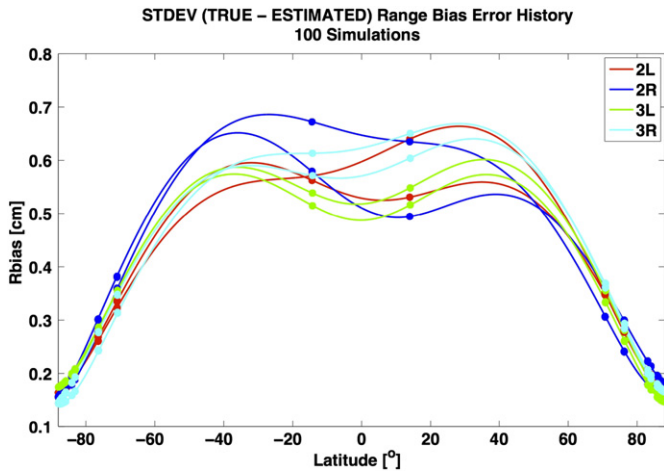


Fig. 9. Potential range bias error (Rbias) as a function of latitude for the beams that are not monitored by the transmitter echo calibration. This is the residual error after the calibration.

The range delay through the atmosphere is a function of the total atmospheric pressure, the partial pressure of water vapor and air temperature. Depending on the atmospheric state, this correction is typically between -2.6 and -0.9 m. ICESat-2 uses the output of NASA's Global Modeling and Assimilation Office GEOS-5 model to determine the state of the atmosphere and calculate the total atmospheric range correction.

Although all heights on ICESat-2 data products are referenced to the WGS-84 ellipsoid, there are several science applications that would benefit from the conversion factor between the ellipsoid and the geoid. ICESat-2 provides such a value to allow heights to be converted to the EGM 2008 geoid model in a mean tide system where the permanent tides are included.

The solid earth and ocean pole tides account for the tidal response of the earth to the centrifugal potential caused by small perturbations of the Earth's rotational axis (i.e. polar motion). The value of these corrections is calculated based on IERS 2010 model conventions. Solid earth pole tides have amplitudes typically on the order of ± 1.5 cm while ocean pole tides have amplitudes typically on the order of ± 0.2 cm.

While several of these geophysical corrections are applied to the photon elevations, the atmospheric path delay correction is applied during the conversion of photon time of flight to range. In addition to these operational corrections, scientists may apply further corrections increasing ICESat-2 precision or accuracy depending on their discipline. Table 2 provides a summary of the geophysical corrections.

3.5. Coverage and operations

ICESat-2 will use a 91-day exact repeat frozen orbit at a 92-degree inclination angle, providing coverage up to 88° North and South generating 1387 ground tracks. It has a nominal orbit altitude of ~500 km.

Table 2

Summary of auxiliary data and geophysical corrections. The Geoid are reference values, but not applied to the product. They are provided for easy comparison. The meteorological data are from the atmospheric correction model.

Model type	Input parameters	Output parameters	Source	Magnitude
Ocean tides	Lat, long, time	Ocean height correction	GOT 4.8	± 5 m
Meteorological data	Lat, long, time	Surface and column temperature, pressure	NASA GMAO GEOS-5	
Inverted barometer/dynamic atmospheric correction	Lat, long, time	Ocean height correction	MOG2D (AVISO)	± 50 cm
Ocean loading	Lat, long, time	Ocean height correction	GOT 4.8	-6 to 0 cm
Solid earth pole tide	Lat, long, time	Solid earth deformation	IERS Conventions (2010)	± 1.5 cm
Ocean pole tide	Lat, long, time	Ocean height correction	IERS Conventions (2010)	± 0.2 cm
Solid earth tides	Lat, long, time	Solid earth deformation	IERS Conventions (2010)	± 40 cm
Geoid	Lat, long	Reference surface	EGM2008, mean tide system	-105 to $+90$ m
Total column atmospheric correction	lat, long, time	Range correction	NASA GMAO GEOS-5	-2.6 to -0.9 m

Since the number of ground tracks and the inclination angle are different compared to ICESat, the ICESat-2 ground tracks do not align with the ICESat ground tracks. However, there are a substantial number of cross-over locations between the ICESat and ICESat-2 ground tracks, particularly in the polar regions, which will enable linking ICESat-2 data to ICESat.

ICESat-2 will collect repeat-track observations for the polar regions. For mid-latitudes operational off-nadir pointing at different angles will generate a dense grid of measurements over a two-year period. These operational maneuvers are in response to the requirement h) in Section 2 that requires a track density of 2 km over two years. At the equator this leads to the following ground track pattern for the first two years of the mission (Fig. 10). This will enable dense sampling of canopy height measurements and thus provide carbon inventory during the first two years of the mission.

Fig. 11 shows one day of reference ground track coverage. The areas in red and blue indicate the transition periods where the satellite changes from the repeat ground track to the "vegetation tracks" and back. Science measurements will be taken at any time during these transitions.

Fig. 12 shows the conceptual mission operations plan. Over the polar regions, the satellite will be in repeat-track mode enabling seasonal repeat measurements. The satellite will point off-nadir over land to generate a dense grid of measurements. While ICESat-2 will generate ocean elevation maps, ICESat-2 will also perform regular calibration maneuvers over the ocean.

4. Instrument, spacecraft, launch vehicle, ground system

The ATLAS instrument is being built at NASA Goddard Space Flight Center and will carry two 532 nm lasers, one operating at a time. The laser energy is adjustable and will be between 48 and 170 μ J per pulse with a nominal energy of 120 μ J for the strong spots and a quarter of it for the weak spots. The pulse width of each laser shot is 1.5 ns and the start pulse is timed at four points over the transmit waveform. Generally the start time will be the average of these four times but the separate measurements allow the monitoring of changes in pulse width and pulse shape symmetry. At the focal plane of the 0.8 m diameter telescope are 6 receiver fibers that send the light through a very narrow (± 19 pm) filter to eliminate most of the sunlight. The remaining photons are then detected by photo-multiplier tubes. ATLAS carries a redundant bank of detectors. More ATLAS parameters are provided in Appendix A.

The spacecraft is being built by Orbital ATK in Gilbert, AZ, and utilizes the heritage from the Landsat-8 satellite, which was also built by Orbital ATK. The spacecraft will carry fuel for a 7-year mission. To enable the required high precision orbit and pointing knowledge the GPS system and star trackers are directly mounted onto the ATLAS optical bench instead of on the spacecraft.

The ICESat-2 Observatory will be launched on board a United Launch Alliance (ULA) Delta II 7420-10 launch vehicle at Vandenberg Air Force Base. The ICESat-2 mission will be the final launch for the Delta II program after >150 launches dating back to 1989.

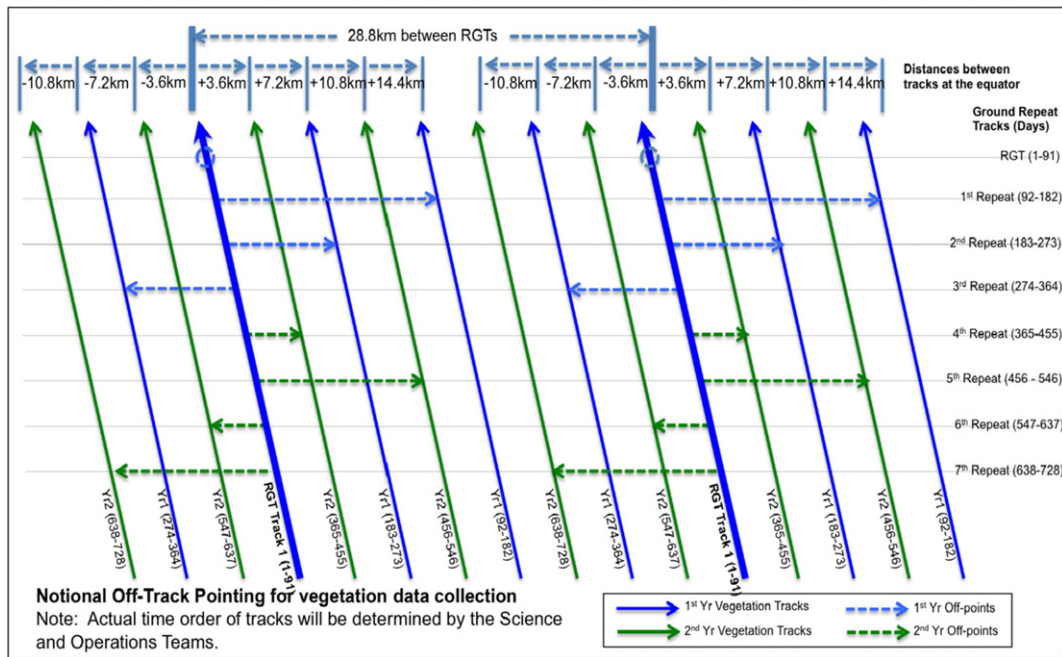


Fig. 10. Ground track pattern at the equator for the first two years of operation. The bold blue lines show the first tracks for the 2-year period. These are the nominal 91-day repeat tracks. At the equator, the gap is 28.8 km. 91 days later the tracks will be shifted by 14.4 km to the right, reducing the gap by half. This halving of the gap will be repeated over two years, i.e. 8 times. The combination of ascending and descending orbits will result in track spacings of <2 km. The maximum off-nadir angle is about 1.5°. (For interpretation of the references to color in this figure legend, the reader is referred to the web version of this article.)

The Mission Operation Center (MOC) will be in Reston, VA with a back-up MOC in Gilbert, AZ. The MOC performs observatory commanding and monitoring throughout the mission lifespan. This includes mission planning and scheduling, monitor and control of the spacecraft, controlling ground communications, and maintaining spacecraft flight software. NASA Goddard Space Flight Center is hosting the Instrument Support Facility (ISF) and the Science Investigator-led Processing System (SIPS). The ISF performs ATLAS mission planning, command, and control, ATLAS health and safety monitoring, and trend analysis of ATLAS operations. It maintains ATLAS flight software and configuration. The SIPS will provide the functions necessary to produce and distribute the routine science data products for the ICESat-2 mission. A complete

list of data products is given in [Appendix B](#). Data products will be sent from the SIPS to the NASA Distributed Active Archive Center (DAAC) at the National Snow and Ice Data Center in Boulder, CO for distribution to the public. The data latency is 2 weeks for the geolocated range and elevation data, and 1 month for the geophysical data after completion of data accumulation required for the specific geophysical products.

5. Summary

ICESat-2 is a 2nd generation space laser altimeter for earth elevation measurements and differs substantially from its ICESat predecessor in concept, technology, data products, and operations compared to ICESat.

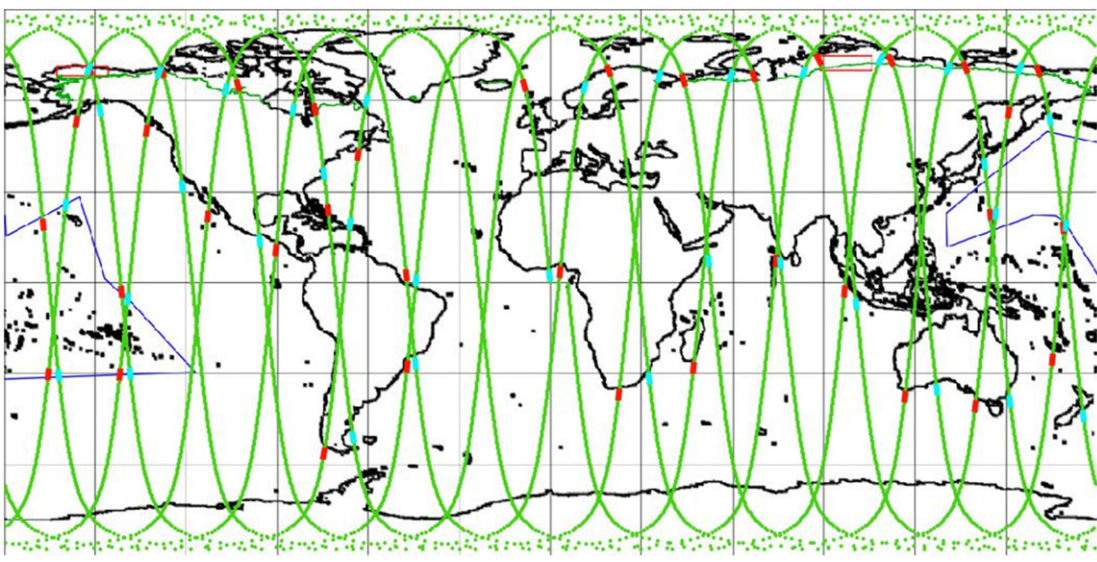


Fig. 11. Illustration of one day of ICESat-2 orbits. The blue and red orbit sections indicate where the pointing transitions from the polar “repeat-track mode” to “land/vegetation mode”, respectively. The transition regions have been defined for all 1387 ground tracks and can be updated on orbit. (For interpretation of the references to color in this figure legend, the reader is referred to the web version of this article.)

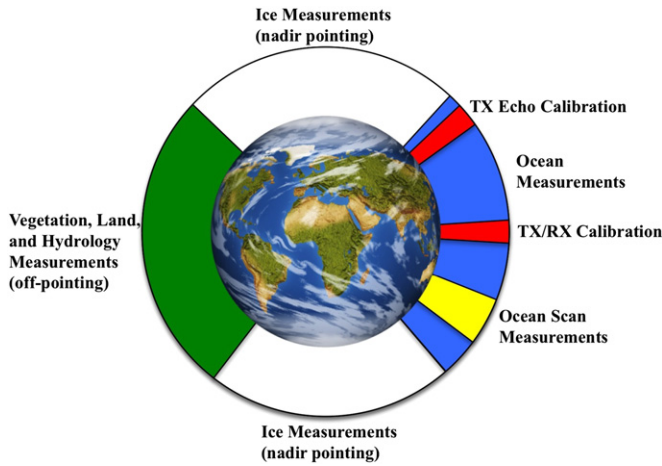


Fig. 12. Conceptual mission operations plan. Calibration efforts will be performed over the ocean. TX Echo Calibration refers to Transmit Echo Calibration described in Section 3.3. Ocean Scan Measurements are also described in Section 3.3. TX/RX calibration corrects the set point of the control loop that keeps the transmitted beam aligned to the receiver field of view.

Lessons learned and scientific findings from ICESat were considered in the design and development of ICESat-2.

The multi-beam approach is central to ICESat-2. This will enable the separation of slope effects from elevation changes on a track-by-track basis and will enable the retrieval of ice sheet elevation changes on a seasonal basis. Given that ICESat operated in 30-day campaign mode, ICESat-2’s three pairs of beams, together with the planned continuous operation, will result in 9 times better coverage. Furthermore, the footprint size and footprint spacing are significantly smaller to optimize elevation retrievals over heterogeneous glaciers and to optimize sea surface height estimates from the, often narrow, leads to enable sea ice freeboard retrievals. Operational off-nadir pointing over land areas will ensure optimum coverage for terrestrial and vegetation sciences. ICESat-2 will be the first time that a photon counting laser altimeter concept is realized on a space-borne platform.

Acknowledgments

We would like to thank Tom Wagner and Richard Slonaker, Program Scientist and Program Executive for ICESat-23 at NASA HQ for their support. We also would like to thank all the members of the project science office for their help. Finally, we would like to thank the reviewers for their thorough reading of the manuscript and constructive comments.

Appendix A. List of key mission parameters

Observatory:	
Orbit inclination and coverage	92°; coverage up to 88° N and S
Track repeat period (polar regions)	91-day exact repeat orbit with monthly sub-cycle for the polar regions and oceans. Operational off-nadir pointing over land areas to generate a dense grid of data over 2 years.
Nominal altitude	500 km
Semi-major axis	6855.9539 km
Pointing control	45 m
Pointing knowledge	6.5 m
Nominal duration of mission	3 years

ATLAS:

Laser wavelength	532 nm
Transmitted pulse width	1.5 ns FWHM
Pulse repetition rate	10 kHz (~0.7 m along-track spacing at nominal altitude)
Number of beams	6 organized in 3 pairs
Beam spacing (across track) at nominal altitude	90 m within pairs
Illuminated spot diameter (85% EE)	3.3 km between pairs
Telescope aperture diameter	<17.5 m at nominal altitude
Receiver field of view diameter	0.8 m
Solar-blocking filter effective width	42.5 m at nominal altitude
Photon-counting detector	38 pm
Receiver dead time, per channel	Hamamatsu photomultiplier with 16 detector elements for strong beams and 4 detector elements for weak beams
Single photon time-of-flight precision	3.2 ± 0.2 ns
Receiver dead time, per channel	800 ps (standard deviation)

MABEL:

Laser wavelength	532 and 1064 nm
Transmitted pulse width	1.5 ns
ER-2 nominal altitude	~20 km (65,000 ft)
Pulse repetition rate	5–25 kHz; operated at 5 kHz (~0.04 m along-track spacing at nominal altitude)
Number of beams	As many as 16 (532 nm) and 8 (1064 nm) beams organized into 2 linear arrays
Total ground swath	~2 km
Footprint size	2 m (at nominal altitude)
Telescope aperture diameter	0.13 m
Receiver field of view diameter	2 m (at nominal altitude)
Photon-counting detector	Hamamatsu model H7260 photomultiplier
Receiver dead time	3 ns
Single photon time-of-flight precision	800 ps (standard deviation)

Appendix B. Overview of the operational ICESat-2 data products. The left column contains the product indicator name.

ATL00	Telemetry data	Raw ATLAS telemetry in packet format
ATL01	Reformatted Telemetry	Parsed, partially reformatted into HDF5, generated daily, segmented into several minute granules.
ATL02	Science Unit Converted Telemetry	Photon time of flight, corrected for instrument effects. Includes all photons, pointing data, spacecraft position, housekeeping data, engineering data, and raw atmospheric profiles, segmented into several minute granules.
ATL03	Global Geolocated Photon Data	Precise latitude, longitude and elevation for every received photon, arranged by beam in the along-track direction. Photons classified by signal vs. background, as well as by surface type (land ice, sea ice, land, ocean), including all geophysical corrections (e.g. Earth tides, atmospheric delay, etc...). Segmented into several minute granules.
ATL04	Uncalibrated Backscatter Profiles	Along-track atmospheric backscatter data, 25 times per second. Includes calibration coefficients for polar regions. Segmented into several minute granules.
ATL06	Land Ice Elevation	Surface height for each beam with along- and across-track slopes calculated for each beam pair. Posted at 40 m along-track; segmented into several minute granules.
ATL07	Arctic/Antarctic Sea Ice Elevation	Height of sea ice and open water leads at varying length scale based on returned photon

(continued on next page)

Appendix B. (continued)

ATL08	Land Water Vegetation Elevation	rate for each beam presented along-track. Height of ground including canopy surface posted at variable length scales relative to signal level, for each beam presented along-track. Where data permits include canopy height, canopy cover percentage, surface slope and roughness, and apparent reflectance.
ATL09	Calibrated Backscatter and Cloud Characteristics	Along-track cloud and other significant atmosphere layer heights, blowing snow, integrated backscatter, and optical depth.
ATL10	Arctic/Antarctic Sea Ice Freeboard	Estimate of sea ice freeboard over specific spatial scales using all available sea surface height measurements. Contains statistics of sea surface and sea ice heights.
ATL11	Antarctica/Greenland Ice Sheet H(t) Series	Time series of height at points on the ice sheet, calculated based on repeat tracks and/or cross-overs.
ATL12	Ocean Elevation	Surface height at specific length scale. Where data permits include estimates of height distribution, roughness, surface slope, and apparent reflectance.
ATL13	Inland Water Height	Along-track inland and near shore water surface height distribution within water mask. Where data permit, include roughness, slope and aspect.
ATL14	Antarctica/Greenland Ice Sheet H(t) Gridded	Height maps of each ice sheet for each year based on all available elevation data.
ATL15	Antarctica/Greenland Ice Sheet dh/dt Gridded	Height change maps for each ice sheet, for each mission year, and for the whole mission.
ALT16	ATLAS Atmosphere Weekly	Polar cloud fraction, blowing snow frequency, ground detection frequency.
ATL17	ATLAS Atmosphere Monthly	Polar cloud fraction, blowing snow frequency, ground detection frequency.
ATL18	Land/Canopy Gridded	Gridded ground surface height, canopy height, and canopy cover estimates.
ATL19	Mean Sea Surface (MSS)	Gridded ocean height product.
ATL20	Arctic/Antarctic Gridded Sea Ice Freeboard	Gridded sea ice freeboard.
ATL21	Arctic/Antarctic Gridded Sea Surface Height w/in Sea Ice	Gridded monthly sea surface height inside the sea ice cover.

References

- Abdalati, W., Zwally, H.J., Bindschadler, R., Csatho, B., Farrell, S.L., Fricker, H.A., Harding, D., Kwok, R., Lefsky, M., Markus, T., Marshak, A., Neumann, T., Palm, S., Schutz, B., Smith, B., Spinhirne, J., Webb, C., 2010. The ICESat-2 laser altimetry mission. *Proc. IEEE* 98 (5):735–751. <http://dx.doi.org/10.1109/JPROC.2009.2034765>.
- Ahmed, R., Siqueira, P., Hensley, S., 2013. A study of forest biomass estimates from LiDAR in the northern temperate forests of New England. *Remote Sens. Environ.* 130, 121–135.
- Bolch, T., Sandberg Sørensen, L., Simonsen, S.B., Mölg, N., Machguth, H., Rastner, P., Paul, F., 2013. Mass loss of Greenland's glaciers and ice caps 2003–2008 revealed from ICESat laser altimetry data. *Geophys. Res. Lett.* 40 (5):875–881. <http://dx.doi.org/10.1002/grl.50270>.
- Brunt, K.M., Fricker, H.A., Padman, L., Scambos, T.A., O'Neil, S., 2010. Mapping the grounding zone of the Ross Ice Shelf, Antarctica, using ICESat laser altimetry. *Ann. Glaciol.* 51 (55):71–79. <http://dx.doi.org/10.3189/172756410791392790>.
- Brunt, K.M., Fricker, H.A., Padman, L., 2011. Analysis of ice plains of the Filchner–Ronne Ice Shelf, Antarctica, using ICESat laser altimetry. *J. Glaciol.* 57 (205):965–975. <http://dx.doi.org/10.3189/002214311798043753>.
- Brunt, K.M., Neumann, T.A., Walsh, K.M., Markus, T., 2014. Determination of local slope on the Greenland Ice Sheet using a multibeam photon-counting Lidar in preparation for the ICESat-2 Mission. *IEEE Geosci. Remote Sens. Lett.* 11 (5):935–939. <http://dx.doi.org/10.1109/LGRS.2013.2282217>.
- Brunt, K.M., Neumann, T.A., Amundson, J.M., Kavanaugh, J.L., Moussavi, M.S., Walsh, K.M., Cook, W.B., Markus, T., 2016. MABEL photon-counting laser altimetry data in Alaska for ICESat-2 simulations and development. *Cryosphere Discuss.*:1–31 <http://dx.doi.org/10.5194/tc-2015-225>.
- Carrère, L., Lyard, F., 2003. Modeling the barotropic response of the global ocean to atmospheric wind and pressure forcing - comparisons with observations. <http://dx.doi.org/10.1029/2002GL016473>.
- Connor, L.N., Farrell, S.L., McAdoo, D.C., Krabill, W.B., Manizade, S., 2013. Validating icesat over thick sea ice in the northern Canada basin. *IEEE Trans. Geosci. Remote Sens.* 51 (4):2188–2200. <http://dx.doi.org/10.1109/TGRS.2012.2211603>.
- Csatho, B.M., Schenk, A.F., van der Veen, C.J., Babonis, G., Duncan, K., Rezvanbehani, S., van den Broeke, M.R., Simonsen, S.B., Nagarajan, S., van Angeland, J.H., 2014. Laser altimetry reveals complex pattern of Greenland Ice Sheet dynamics. *Proc. Natl. Acad. Sci.* 111 (52):18478–18483. <http://dx.doi.org/10.1073/pnas.1411680112>.
- Farrell, S.L., Laxon, S.W., McAdoo, D.C., Yi, D., Zwally, H.J., 2009. Five years of Arctic sea ice freeboard measurements from the ice, cloud and land elevation satellite. *J. Geophys. Res. Oceans* 114 (C4). <http://dx.doi.org/10.1029/2008JC005074>.
- Farrell, S.L., McAdoo, D.C., Laxon, S.W., Zwally, H.J., Yi, D., Ridout, A., Giles, K., 2012. Mean dynamic topography of the Arctic Ocean. *Geophys. Res. Lett.* 39 (1). <http://dx.doi.org/10.1029/2011GL050052>.
- Farrell, S.L., Brunt, K.M., Ruth, J.M., Kuhn, J.M., Connor, L.N., Walsh, K.M., 2015. Sea-ice freeboard retrieval using digital photon-counting laser altimetry. *Ann. Glaciol.* 56 (69):167–174. <http://dx.doi.org/10.3189/2015AoG69A686>.
- Fricker, H.A., Scambos, T., Bindschadler, R., Padman, L., 2007. An active subglacial water system in West Antarctica mapped from space. *Science* 315 (5818):1544–1548. <http://dx.doi.org/10.1126/science.1136897>.
- Fricker, H.A., Coleman, R., Padman, L., Scambos, T.A., Bohlander, J., Brunt, K.M., 2009. Mapping the grounding zone of the Amery Ice Shelf, East Antarctica using InSAR, MODIS and ICESat. *Antarct. Sci.* 21 (05):515–532. <http://dx.doi.org/10.1017/S095410200999023X>.
- Gardner, A.S., Moholdt, G., Wouters, B., Wolken, G.J., Burgess, D.O., Sharp, M.J., Cogley, J.G., Braun, C., Labine, C., 2011. Sharply increased mass loss from glaciers and ice caps in the Canadian Arctic Archipelago. *Nature* 473 (7347):357–360. <http://dx.doi.org/10.1038/nature10089>.
- Gardner, A., Moholdt, G., Arendt, A., Wouters, B., 2012. Accelerated contributions of Canada's Baffin and Bylot Island glaciers to sea level rise over the past half century. *Cryosphere* 6 (5):1103–1125. <http://dx.doi.org/10.5194/tc-6-1103-2012>.
- Gardner, A.S., Moholdt, G., Cogley, J.G., Wouters, B., Arendt, A.A., Wahr, J., Berthier, E., Hock, R., Pfeffer, W.T., Kaser, G., Ligtenberg, S.R.M., Bolch, T., Sharp, M.J., Hagen, J.O., van den Broeke, M.R., Paul, F., 2013. A reconciled estimate of glacier contributions to sea level rise: 2003 to 2009. *Science* 340 (6134):852–857. <http://dx.doi.org/10.1126/science.1234532>.
- Glenn, N.F., Neuenschwander, A., Vierling, L.A., Spaete, L., Li, A., Shinneman, D.J., Pilliod, D.S., Arkle, R.S., McLroy, S.K., 2016. Landsat 8 and ICESat-2: Performance and potential synergies for quantifying dryland ecosystem vegetation cover and biomass. *Remote Sens. Environ.* <http://dx.doi.org/10.1016/j.rse.2016.02.039>.
- Groh, A., Ewert, H., Scheinert, M., Fritsche, M., Rülke, A., Richter, A., Rosenau, R., Dietrich, R., 2012. An investigation of glacial isostatic adjustment over the Amundsen Sea Sector, West Antarctica. *Glob. Planet. Chang.* 98:45–53. <http://dx.doi.org/10.1016/j.gloplacha.2012.08.001>.
- Gunter, B., Urban, T., Riva, R., Helsen, M., Harpole, R., Poole, S., Nagel, P., Schutz, B., Tapley, B., 2009. A comparison of coincident GRACE and ICESat data over Antarctica. *J. Geod.* 83 (11):1051–1060. <http://dx.doi.org/10.1007/s00190-009-0323-4>.
- Gwenzi, D., Lefsky, M.A., 2014. Prospects of photon counting lidar for savanna ecosystem structural studies. *Int. Arch. Photogramm. Remote. Sens. Spat. Inf. Sci.* 40 (1):141. <http://dx.doi.org/10.5194/isprsarchives-XL-1-141-2014>.
- Haran, T., Bohlander, J., Scambos, T., Fahnestock, M., 2005. *Compilers: MODIS mosaic of Antarctica (MOA) image map: Digital media. National Snow and Ice Data Center, Boulder, CO, USA.*
- Harding, D.J., Carabajal, C.C., 2005. ICESat waveform measurements of within-footprint topographic relief and vegetation vertical structure. *Geophys. Res. Lett.* 32 (21). <http://dx.doi.org/10.1029/2005GL023971>.
- Hay, C.C., Morrow, E., Kopp, R.E., Mitrovica, J.X., 2015. Probabilistic reanalysis of twentieth-century sea-level rise. *Nature* 517 (7535):481–484. <http://dx.doi.org/10.1038/nature14093>.
- Herzfeld, U.C., McDonald, B.W., Wallin, B.F., Neumann, T.A., Markus, T., Brenner, A., Field, C., 2014. Algorithm for detection of ground and canopy cover in micropulse photon-counting lidar altimeter data in preparation for the ICESat-2 mission. *IEEE Trans. Geosci. Remote Sens.* on 52 (4):2109–2125. <http://dx.doi.org/10.1109/TGRS.2013.2258350>.
- Houghton, R.A., 2005. Aboveground forest biomass and the global carbon balance. *Glob. Chang. Biol.* 11 (6):945–958. <http://dx.doi.org/10.1111/j.1365-2486.2005.00955.x>.
- Howat, I.M., Smith, B.E., Joughin, I., Scambos, T.A., 2008. Rates of southeast Greenland ice volume loss from combined ICESat and ASTER observations. *Geophys. Res. Lett.* 35 (17). <http://dx.doi.org/10.1029/2008GL034496>.
- Jasinski, M. F., Stoll, J. D., Cook, W. B., Ondrusek, M., Stengel, E., & Brunt, K.M. (2016, accepted). Inland and near shore water profiles derived from the high altitude Multiple Altimeter Beam Experimental Lidar (MABEL). *J. Coast. Res.*
- Kääb, A., Berthier, E., Nuth, C., Gardelle, J., Arnaud, Y., 2012. Contrasting patterns of early twenty-first-century glacier mass change in the Himalayas. *Nature* 488 (7412):495–498. <http://dx.doi.org/10.1038/nature11324>.
- Khan, S.A., Kjør, K.H., Bevis, M., Bamber, J.L., Wahr, J., Kjeldsen, K.K., Björk, A.A., Korsgaard, N.J., Stearns, L.A., van den Broeke, M.R., Liu, L., Larsen, N.K., Muresan, J.S., 2014. Sustained mass loss of the northeast Greenland ice sheet triggered by regional warming. *Nat. Clim. Chang.* 4 (4):292–299. <http://dx.doi.org/10.1038/nclimate2161>.
- Krankina, O.N., Harmon, M.E., Schnekenburger, F., Sierra, C.A., 2012. Carbon balance on federal forest lands of Western Oregon and Washington: the impact of the Northwest Forest Plan. *For. Ecol. Manag.* 286, 171–182.
- Kuipers Munneke, P., Ligtenberg, S., Noël, B.P.Y., Howat, I.M., Box, J.E., Mosley-Thompson, E., McConnell, J.R., Steffen, K., Harper, J.T., Das, S.B., Van Den Broeke, M.R., 2015. Elevation change of the Greenland Ice Sheet due to surface mass balance and firn processes, 1960–2014. *Cryosphere* 9 (6):2009–2025. <http://dx.doi.org/10.5194/tc-9-2009-2015>.
- Kurtz, N.T., Markus, T., 2012. Satellite observations of Antarctic sea ice thickness and volume. *J. Geophys. Res. Oceans* 117 (C8). <http://dx.doi.org/10.1029/2012JC008141>.
- Kwok, R., Rothrock, D.A., 2009. Decline in Arctic sea ice thickness from submarine and ICESat records: 1958–2008. *Geophys. Res. Lett.* 36 (15). <http://dx.doi.org/10.1029/2009GL039035>.

- Kwok, R., Cunningham, G.F., Wensnahan, M., Rigor, I., Zwally, H.J., Yi, D., 2009. Thinning and volume loss of the Arctic Ocean sea ice cover: 2003–2008. *J. Geophys. Res. Oceans* 114 (C7). <http://dx.doi.org/10.1029/2009JC005312>.
- Kwok, R., Markus, T., Morison, J., Palma, S.P., Neumann, T.A., Brunt, K.M., Cook, W.B., Hancock, D.W., Cunningham, G.F., 2014. Profiling sea ice with a multiple altimeter beam experimental lidar (MABEL). <http://dx.doi.org/10.1175/JTECH-D-13-00120.1>.
- Laxon, S.W., Giles, K.A., Ridout, A.L., Wingham, D.J., Willatt, R., Cullen, R., Kwok, R., Schweiger, A., Zhang, J., Haas, C., Hendricks, S., Krishfield, R., Kurtz, N., Farrell, S.L., Davidson, M., 2013. CryoSat-2 estimates of Arctic sea ice thickness and volume. *Geophys. Res. Lett.* 40 (4):732–737. <http://dx.doi.org/10.1002/grl.50193>.
- Le Quéré, C., et al., 2015. Global Carbon Budget. :p. 2014 <http://dx.doi.org/10.5194/essd-7-47-2015>.
- Lefsky, M.A., 2010. A global forest canopy height map from the Moderate Resolution Imaging Spectroradiometer and the Geoscience Laser Altimeter System. *Geophys. Res. Lett.* 37 (15). <http://dx.doi.org/10.1029/2010GL043622>.
- Lefsky, M.A., Keller, M., Pang, Y., De Camargo, P.B., Hunter, M.O., 2007. Revised method for forest canopy height estimation from Geoscience Laser Altimeter System waveforms. *J. Appl. Remote Sens.* 1 (1). http://dx.doi.org/10.1117/1.2795724_013537-013537.
- Ligtenberg, S.R.M., Horwath, M., den Broeke, M.R., Legréy, B., 2012. Quantifying the seasonal “breathing” of the Antarctic ice sheet. *Geophys. Res. Lett.* 39 (23). <http://dx.doi.org/10.1029/2012GL053628>.
- Loomis, B.D., Luthcke, S.B., 2014. Optimized signal denoising and adaptive estimation of seasonal timing and mass balance from simulated GRACE-like regional mass variations. *Adv. In Adap. Data Anal.* 6 (1). <http://dx.doi.org/10.1142/S1793536914500034>.
- Los, S.O., Rosette, J.A.B., Kljun, N., North, P.R.J., Chasmer, L., Suárez, J.C., Hopkinson, C., Hill, R.A., van Gorsel, E., Mahoney, C., Berni, J.A.J., 2012. Vegetation height and cover fraction between 60 S and 60 N from ICESat GLAS data. *Geosci. Model Dev.* 5 (2): 413–432. <http://dx.doi.org/10.5194/gmd-5-413-2012>.
- Luthcke, S.B., Rowlands, D.D., McCarthy, J.J., Pavlis, D.E., Stoneking, E., 2000. Spaceborne laser-altimeter-pointing bias calibration from range residual analysis. *J. Spacecr. Rocket.* 37 (3):374–384. <http://dx.doi.org/10.2514/2.3571>.
- Luthcke, S.B., Rowlands, D.D., Williams, T.A., Sirota, M., 2005. Reduction of ICESat systematic geolocation errors and the impact on ice sheet elevation change detection. *Geophys. Res. Lett.* 32 (21). <http://dx.doi.org/10.1029/2005GL023689>.
- Luthcke, S.B., Sabaka, T.J., Loomis, B.D., Arendt, A.A., McCarthy, J.J., Camp, J., 2013. Antarctica, Greenland and Gulf of Alaska land ice evolution from an iterated GRACE global mascon solution. *J. Glaciol.* 59 (216). <http://dx.doi.org/10.3189/2013jgl012j147>.
- McAdoo, D.C., Farrell, S.L., Laxon, S., Ridout, A., Zwally, H.J., Yi, D., 2013. Gravity of the Arctic Ocean from satellite data with validations using airborne gravimetry: oceanographic implications. *J. Geophys. Res. Oceans* 118 (2):917–930. <http://dx.doi.org/10.1002/jgrc.20080>.
- McGill, M., Markus, T., Scott, V.S., Neumann, T., 2013. The multiple altimeter beam experimental Lidar (MABEL): An airborne simulator for the ICESat-2 mission. *J. Atmos. Ocean. Technol.* 30 (2):345–352. <http://dx.doi.org/10.1175/JTECH-D-12-00076.1>.
- Moholdt, G., Nuth, C., Hagen, J.O., Kohler, J., 2010. Recent elevation changes of Svalbard glaciers derived from ICESat laser altimetry. *Remote Sens. Environ.* 114 (11): 2756–2767. <http://dx.doi.org/10.1016/j.rse.2010.06.008>.
- Moholdt, G., Wouters, B., Gardner, A.S., 2012. Recent mass changes of glaciers in the Russian High Arctic. *Geophys. Res. Lett.* 39 (10). <http://dx.doi.org/10.1029/2012gl051466>.
- Neuenschwander, A.L., Urban, T.J., Gutierrez, R., Schutz, B.E., 2008. Characterization of ICESat/GLAS waveforms over terrestrial ecosystems: implications for vegetation mapping. *J. Geophys. Res. Biogeosci.* 113 (G2). <http://dx.doi.org/10.1029/2007JG000557>.
- Padman, L., Erofeeva, S.Y., Fricker, H.A., 2008. Improving Antarctic tide models by assimilation of ICESat laser altimetry over ice shelves. *Geophys. Res. Lett.* 35 (22). <http://dx.doi.org/10.1029/2008GL035592>.
- Price, S.F., Payne, A.J., Howat, I.M., Smith, B.E., 2011. Committed sea-level rise for the next century from Greenland ice sheet dynamics during the past decade. *Proc. Natl. Acad. Sci.* 108 (22):8978–8983. <http://dx.doi.org/10.1073/pnas.1017313108>.
- Pritchard, H.D., Arthern, R.J., Vaughan, D.G., Edwards, L.A., 2009. Extensive dynamic thinning on the margins of the Greenland and Antarctic ice sheets. *Nature* 461 (7266): 971–975. <http://dx.doi.org/10.1038/nature08471>.
- Pritchard, H.D., Ligtenberg, S.R.M., Fricker, H.A., Vaughan, D.G., Van den Broeke, M.R., Padman, L., 2012. Antarctic ice-sheet loss driven by basal melting of ice shelves. *Nature* 484 (7395):502–505. <http://dx.doi.org/10.1038/nature10968>.
- Ray, R.D., 2008. A preliminary tidal analysis of ICESat laser altimetry: Southern Ross Ice Shelf. *Geophys. Res. Lett.* 35 (2). <http://dx.doi.org/10.1029/2007GL032125>.
- Rothrock, D.A., Percival, D.B., Wensnahan, M., 2008. The decline in arctic sea-ice thickness: separating the spatial, annual, and interannual variability in a quarter century of submarine data. *J. Geophys. Res. Oceans* 113 (C5). <http://dx.doi.org/10.1029/2007JC004252>.
- Sasgen, I., van den Broeke, M., Bamber, J.L., Rignot, E., Sørensen, L.S., Wouters, B., Martinec, Z., Velicogna, I., Simonsen, S.B., 2012. Timing and origin of recent regional ice-mass loss in Greenland. *Earth Planet. Sci. Lett.* 333:293–303. <http://dx.doi.org/10.1016/j.epsl.2012.03.033>.
- Schutz, B.E., Zwally, H.J., Shuman, C.A., Hancock, D., DiMarzio, J.P., 2005. Overview of the ICESat mission. *Geophys. Res. Lett.* 32 (21). <http://dx.doi.org/10.1029/2005GL024009>.
- Shepherd, A., Ivins, E.R., A. G., Barletta, V.R., Bentley, M.J., Bettadpur, S., Briggs, K.H., Bromwich, D.H., Forsberg, R., Galin, N., Horwath, M., Jacobs, S., Joughin, I., King, M.A., Lenaerts, J.T.M., Li, J., Ligtenberg, S.R.M., Luckman, A., Luthcke, S.B., McMillan, M., Meister, R., Milne, G., Mougnot, J., Muir, A., Nicolas, J.P., Paden, J., Payne, A.J., Pritchard, H., Rignot, E., Rott, H., Sorensen, L.S., Scambos, T.A., Scheuchl, B., Schrama, E.J.O., Smith, B., Sundal, A.V., van Angelen, J.H., van de Berg, W.J., van den Broeke, M.R., Vaughan, D.G., Velicogna, I., Wahr, J., Whitehouse, P.L., Wingham, D.J., Yi, D., Young, D., Zwally, H.J., 2012. A reconciled estimate of ice-sheet mass balance. *Science* 338 (6111):1183–1189. <http://dx.doi.org/10.1126/science.1228102>.
- Simard, M., Pinto, N., Fisher, J.B., Baccini, A., 2011. Mapping forest canopy height globally with spaceborne lidar. *J. Geophys. Res. Biogeosci.* 116 (G4). <http://dx.doi.org/10.1029/2011JG001708>.
- Smith, B.E., Fricker, H.A., Joughin, I.R., Tulaczyk, S., 2009. An inventory of active subglacial lakes in Antarctica detected by ICESat (2003–2008). *J. Glaciol.* 55 (192):573–595. <http://dx.doi.org/10.3189/002214309789470879>.
- Sørensen, L.S., Simonsen, S.B., Nielsen, K., Lucas-Picher, P., Spada, G., Adalgeirsdottir, G., Forsberg, R., Hvidberg, C., 2011. Mass balance of the Greenland ice sheet (2003–2008) from ICESat data—the impact of interpolation, sampling and firn density. *Cryosphere* 5:173–186. <http://dx.doi.org/10.5194/tc-5-173-2011>.
- Spinhirne, J.D., Palm, S.P., Hart, W.D., Hlavka, D.L., Welton, E.J., 2005. Cloud and aerosol measurements from GLAS: overview and initial results. *Geophys. Res. Lett.* 32 (22). <http://dx.doi.org/10.1029/2005GL023507>.
- Stammer, D., Ray, R.D., Andersen, O.B., Arbic, B.K., Bosch, W., Carrère, L., Cheng, Y., Chinn, D.S., Dushaw, B.D., Egbert, G.D., Erofeeva, S.Y., Fok, H.S., Green, J.A.M., Griffiths, S., King, M.A., Lapin, V., Lemoine, F.G., Luthcke, S.B., Lyard, F., Morison, J., Müller, M., Padman, L., Richman, J.G., Shriver, J.F., Shum, C.K., Taguchi, E., Yi, Y., 2014. Accuracy assessment of global barotropic ocean tide models. *Rev. Geophys.* 52 (3):243–282. <http://dx.doi.org/10.1002/2014RG000450>.
- Stammes, K., Tsay, S.C., Wiscombe, W., Jayaweera, K., 1988. Numerically stable algorithm for discrete-ordinate-method radiative transfer in multiple scattering and emitting layered media. *Appl. Opt.* 27 (12):2502–2509. <http://dx.doi.org/10.1364/AO.27.002502>.
- Thomas, R., Frederick, E., Krabill, W., Manizade, S., Martin, C., 2009. Recent changes on Greenland outlet glaciers. *J. Glaciol.* 55 (189):147–162. <http://dx.doi.org/10.3189/002214309788608958>.
- Urban, T.J., Schutz, B.E., 2005. ICESat sea level comparisons. *Geophys. Res. Lett.* 32 (23). <http://dx.doi.org/10.1029/2005GL024306>.
- Urban, T.J., Schutz, B.E., Neuenschwander, A.L., 2008. A survey of ICESat coastal altimetry applications: continental coast, open ocean island, and inland river. *Terr. Atmos. Ocean. Sci.* 19. [http://dx.doi.org/10.3319/TAO.2008.19.1-2.1\(SA\)](http://dx.doi.org/10.3319/TAO.2008.19.1-2.1(SA)).
- Zwally, H.J., Jun, L.L., Brenner, A.C., Beckley, M., Cornejo, H.G., DiMarzio, J., Giovinetto, M.B., Neumann, T.A., Robbins, J., Saba, J.L., Yi, D., Wang, W., 2011. Greenland ice sheet mass balance: distribution of increased mass loss with climate warming; 2003–07 versus 1992–2002. *J. Glaciol.* 57 (201):88–102. <http://dx.doi.org/10.3189/002214311795306682>.
- Zwally, H.J., Li, J., Robbins, J.W., Saba, J.L., Yi, D., Brenner, A.C., 2015. Mass gains of the Antarctic ice sheet exceed losses. *J. Glaciol.* 61 (230):1019–1036. <http://dx.doi.org/10.3189/2015jgl015j071>.